THE JOURNAL OF COMPARATIVE NEUROLOGY 348:261–276 (1994)

Physiology and Morphology of Complex Spiking Neurons in the Guinea Pig Dorsal Cochlear Nucleus

PAUL B. MANIS, GEORGE A. SPIROU, DEBORA D. WRIGHT, SUSSAN PAYDAR, AND DAVID K. RYUGO
Departments of Otolaryngology-Head and Neck Surgery, Neuroscience and Biomedical Engineering, The Center for Hearing Sciences, The Johns Hopkins University School of Medicine, Baltimore, Maryland 21205

ABSTRACT

Intracellular recordings from the dorsal cochlear nucleus have identified cells with both simple and complex action potential waveforms. We investigated the hypothesis that cartwheel cells are a specific cell type that generates complex action potentials, based on their analogous anatomical, developmental, and biochemical similarities to cerebellar Purkinje cells, which are known to discharge complex action potentials. Intracellular recordings were made from a brain slice preparation of the guinea pig dorsal cochlear nucleus. A subpopulation of cells discharged a series of two or three action potentials riding on a slow depolarization as an all-or-none event; this discharge pattern is called a complex spike or burst. These cells also exhibited anodal break bursts, anomalous rectification, subthreshold inward rectification, and frequent inhibitory postsynaptic potentials (IPSPs). Seven complex-spiking cells were stained with intracellular dyes and subsequently identified as cartwheel neurons. In contrast, six identified simple-spiking cells recorded in concurrent experiments were pyramidal cells.

The cartwheel cell bodies reside in the lower part of layer 1 and the upper part of layer 2 of the nucleus. The cells are characterized by spiny dendrites penetrating the molecular layer, a lack of basal dendritic processes, and an axonal plexus invading layers 2 and 3, and the inner regions of layer 1. The cartwheel cell axons made putative synaptic contacts at the light microscopic level with pyramidal cells and small cells, including stellate cells, granule cells, and other cartwheel cells in layers 1 and 2. The axonal plexus of individual cartwheel cells suggests that they can inhibit cells receiving input from either the same or adjacent parallel fibers and that this inhibition is distributed along the isofrequency contours of the nucleus.

Key words: auditory system, hearing, electrophysiology, intracellular recording, dye staining

One of the distinguishing features of the dorsal cochlear nucleus (DCN) is its diversity of cell types, the majority of which are intrinsic neurons that create an intricate local neuronal circuit. The most numerous interneuronal populations are the cartwheel cells and the granule cells; both of these cell types are involved in circuits that terminate on the principal neurons of the nucleus, the pyramidal cells. The cartwheel cells are found in the molecular and granular layers of the nucleus and share many anatomical and immunocytochemical features with cerebellar Purkinje cells. They are part of a cerebellar-like circuit located within the cochlear nucleus and receive their main excitatory input from parallel fibers arising from cochlear nucleus granule cells. Cartwheel cells are immunoreactive for gamma-aminobutyric acid (GABA; Wenthold et al., 1986; Peyret et al., 1986; Kolston et al., 1992), glutamic acid decarboxylase (GAD; Mugnaini, 1985), glycine (Wenthold et al., 1987; Kolston et al., 1992), the putative calcium binding protein PEP-19 (Berrebi and Mugnaini, 1991), a subunit of the metabotropic glutamate receptor (Petralia et al., 1993; Wright et al., 1993), and cerebellin (Mugnaini and Morgan, 1987). Small neurons assumed to be cartwheel cells are immunolabeled by antibodies to protein kinase C (Saito et al., 1988), the inositol triphosphate receptor (Mignery et al., 1989; Ryugo et al., 1992), and the peptide L7, each of which

Accepted April 20, 1994.

Dr. G. Spirou is now at the Department of Otolaryngology, West Virginia University, Morgantown, WV 26506-9200.

Address reprint requests to Paul B. Manis, Department of Otolaryngology-Head and Neck Surgery, Johns Hopkins University School of Medicine, 420 Ross Research Building, 720 Rutland Avenue, Baltimore, MD 21205.

is also found in high concentration in Purkinje cells. PEP-19 and L7 stain few other cell types in the brain and so have been used as specific markers for cartwheel neurons (Berrebi and Mugnaini, 1991) and as support for a common developmental lineage of the two cell types (Berrebi et al., 1990). Cartwheel neurons also share with Purkinje cells a high dendritic spine density (Wouterlood and Mugnaini, 1984) and, at least in guinea pigs, a polar orientation of the dendrites toward the ependymal surface (Hackney et al., 1990).

On the other hand, cartwheel cells and Purkinje cells exhibit some differentiating features. Each Purkinje cell receives innervation from a climbing fiber, but climbing fiber innervation of cartwheel cells has yet to be reported, in spite of extensive anatomical study. Furthermore, cartwheel cells are immunocytochemically positive for glycine as well as GABA (and GAD), suggesting that they may use either or both amino acids as their neurotransmitter, whereas Purkinje cells label only for GABA (GAD) and appear to use GABA as their principal neurotransmitter. Finally, a cyclic guanosine monophosphate (cGMP)-dependent protein kinase found in abundance in Purkinje cells is only weakly expressed by cartwheel cells (DeCamilli et al., 1984).

Nevertheless, the morphological, biochemical, and developmental similarities between cartwheel neurons and Purkinje cells suggest that these separate cell types may share physiological characteristics through a developmentally regulated expression of similar sets of ion channels. Complex action potential bursts are characteristic of cerebellar Purkinje cells and are, in part, generated by dendritic calcium conductances (Llinas and Nicholson, 1971; Llinas and Sugimori, 1980; Sugimori and Llinas, 1990; Ross et al., 1990; Lev-Ram et al., 1992). In previous intracellular studies of the DCN, a population of cells exhibiting complex action potentials has been recorded in DCN slices (Hirsch and Oertel, 1988; Manis, 1990) but these cells were not morphologically identified. More recently, Zhang and Oertel (1993a) reported on a population of complex spiking cells in the young mouse that they identified as cartwheel cells. In the present study, we investigated the hypothesis that complex spiking cells in the guinea pig DCN are cartwheel neurons. Preliminary results of these studies have been reported in abstract form (Spirou et al., 1991; Manis et al., 1993).

MATERIALS AND METHODS

Slice preparation

Slices from guinea pig brain were prepared as previously described (Manis, 1990). Briefly, pigmented guinea pigs weighing 200–700 g (>1 month old) were anesthetized with pentobarbital (35 mg/kg) and decapitated, and the brainstem was quickly removed. Brain slices 350 μm thick were cut through the dorsal cochlear nucleus with an oscillating tissue slicer. Slices were prepared either parallel to the strial axis (see Manis, 1989) or orthogonal to this plane, in the transstrial axis (Blackstad et al., 1984). The latter plane is approximately parallel to the isofrequency planes of the nucleus. The slices were incubated for 1–2 hours before transfer to the recording chamber. Slices were prepared in a HEPES-buffered solution containing (in mM) 134 NaCl, 5 KCl, 1.25 KH_2PO_4, 10 glucose, 10 HEPES buffer, 0.2 $CaCl_2$, and 4.0 $MgSO_4$, pH 7.35, and equilibrated with 100% O_2 at 22°C. The incubation and recording medium contained (in mM) 130 NaCl, 3 KCl, 1.25 KH_2PO_4, 20 $NaHCO_3$, 10 glucose, 2.5 $CaCl_2$, and 1.3 $MgSO_4$, pH 7.35–7.4, and was equilibrated with 95% O_2-5% CO_2 at 34°C.

Recordings

The recording system and data collection protocols have been described previously (Manis, 1990). Intracellular recordings were made with fine-tipped glass micropipets filled with 3 M potassium acetate and 5 mM potassium chloride, or 3 M potassium chloride, 40–80 MΩ resistance. In some experiments, cells were marked for morphological identification using one of three different dyes (see below): Lucifer yellow CH, neurocytin, or horseradish peroxidase (HRP). Lucifer yellow, neurocytin, and HRP-filled pipets had resistances of 80–150 MΩ. Electrodes were advanced into the DCN under visual control. One advantage of the guinea pig DCN for this study is its highly laminar organization (Berrebi and Mugnaini, 1991; Hackney et al., 1990), and the concentration of cartwheel cells within the deeper part of layer 1 and the upper part of layer 2. We used this knowledge to optimize the probability of cartwheel cell impalement during intracellular recordings by directing our electrodes into the region where the cells are most numerous. The boundary between these layers is clearly visible in transilluminated slices as a difference in the light scattering produced by different densities of myelinated fibers in each layer.

Intracellular injections and histology

Lucifer yellow. Four percent Lucifer yellow CH (Sigma) was dissolved in 0.25 M lithium chloride. Lucifer yellow was injected into cells using 2 nA negative current pulses of 250 msec duration at a rate of 3 Hz. Each negative pulse was followed by a 1 nA positive step for 83 msec. Three to six hours later, the slice was immersed in 5% formalin with 5% dextrose in a 0.15 M phosphate-buffered saline (PBS) for fixation. After 24–48 hours, the slice was rinsed and immersed in a drop of dimethyl sulfoxide on a coverslip (Grace and Llinas, 1985), viewed using epifluorescent illumination, and photographed. The slices were then rinsed in PBS and stored in the dark in fixative. Up to 6 months later (and, for one cell, 2 years later), the slices were embedded in a gelatin-albumin solution hardened with glutaraldehyde, and 50 μm sections were cut on a vibratome. The sections were collected in 50 mM Tris-buffered saline (TBS) and placed in the primary antibody (Molecular Probes, Eugene, OR; rabbit anti-Lucifer yellow) at a dilution of 1:500 in 1% normal goat serum, 0.2% bovine serum albumin (BSA), 1% Triton X-100 in 0.05 M TBS for 42 hours at 5°C on a rotating shaker. The tissue was briefly rinsed in 50 mM Tris buffer and incubated with goat anti-rabbit IgG conjugated to HRP (Vector Labs, Burlingame, CA), diluted 1:500 in the same diluent as used for the primary antibody, for 2 hours at room temperature. Tissue was washed in TBS, incubated for 20 minutes in 0.025% diaminobenzidine (DAB) in 0.1 M TBS (pH 7.6), reacted for 25 minutes in fresh DAB solution with 0.002% H_2O_2, rinsed in TBS, counterstained with 0.5% cresyl violet, dehydrated, and coverslipped in Permount.

Neurocytin. Neurocytin (Vector Labs), 4%, was dissolved in 0.5 M KAc, 50 mM Tris, pH 7.4 (Horikawa and Armstrong, 1988). The dye was injected into cells using 2 nA positive current pulses, 250 msec in duration, at 3 Hz for 5–20 minutes. One to six hours after the injection, slices

were immersed in a solution of 4% paraformaldehyde in 0.1 M phosphate buffer (pH 7.4) overnight at 5°C. Slices with injected cells were embedded in gelatin-albumin, cut on a Vibratome into 50 μm sections, rinsed in TBS, and incubated for 4 hours in a standard ABC solution (Vector Labs). Sections were rinsed again in TBS and reacted using DAB and counterstained as described above.

Horseradish peroxidase. Electrodes contained a solution of 4% HRP (Sigma Type VI) in 0.5 M KCl, 50 mM Tris, pH 7.6. HRP was injected into cells using 2–4 nA positive current pulses, 250 msec in duration, at 3 Hz for 5–20 minutes. Three to six hours later, slices were immersed in a solution of 4% paraformaldehyde in 0.1 M phosphate buffer (pH 7.4) overnight at 5°C. Slices with injected cells were embedded in gelatin-albumin, cut on a Vibratome into 50 μm sections, rinsed in TBS, and reacted using diaminobenzidine (DAB) and counterstained as described above.

Microscopic analysis

All seven stained cells exhibiting complex spikes, and five of six cells exhibiting simple spikes were drawn and analyzed with the aid of a light microscope and drawing tube. (The one cell that was not drawn exhibited apical and basal dendrites typical of pyramidal cells, but the neurocytin labeling was too faint to reconstruct the entire dendritic arborization with confidence.) Cells were reconstructed at a total magnification of ×1,000 (×40 oil-immersion objective, NA 1.0) or ×2,500 (×100 oil-immersion objective, NA 1.25). Individual neurons with their axonal and dendritic arborization extended across multiple sections within a single slice but were pieced together by matching the cut ends of labeled processes on adjacent tissue surfaces. Labeled cells were characterized with respect to the size, shape, and location of their cell bodies; the presence or absence of basal dendrites, amount of dendritic branching; and the nature of dendritic spines. The cell bodies of counterstained neurons that abutted axonal swellings were also drawn and identified on the basis of size, shape and location, shape and position of their nuclei and cytoplasmic staining features (see, e.g., Osen, 1969; Hackney et al., 1990). Pyramidal cells were identified by their relatively large elongated cell body with a central nucleus and clumped cytoplasmic Nissl substance. Granule cells were identified by their small size and relatively round nucleus with a single prominent nucleolus and little cytoplasm. Stellate cells were identified as small cells, of round or ovoid shape, with a relatively large nucleus, prominent nucleolus, and the presence of thin dendritic processes leaving the cell body. Cartwheel cells were identified as medium-sized round cells, approximately 15 μm in diameter, with a centrally placed nucleus and pale cytoplasm. Cartwheel cells have a distinct nuclear indentation (see, e.g., Wouterlood and Mugnaini, 1984) that was frequently visible and used as an identifying criterion. The long axis diameter (mean ± S.D.) of the cell body was determined by measuring the longest dimension passing through the nucleus, and the short axis diameter was represented by the longest dimension passing through the nucleus perpendicular to the long axis.

The populations of physiologically characterized and stained cells were compared to populations of cartwheel and pyramidal cells identified on the basis of cytologic criteria (Hackney et al., 1990). Unlabeled cells were selected and analyzed from the same tissue in which intracellularly stained cells were recovered. Cartwheel cells from additional animals were also identified on the basis of their selective immunoreactivity against the inositol 1,4,5-triphosphate receptor antibody (Ryugo et al., 1992) and measured as described above.

RESULTS

Recordings were made from 29 complex spiking neurons in the DCN. Seven complex spiking cells and six simple spiking cells were successfully and unambiguously stained with dyes for morphological evaluation. Twelve of the complex spiking cells were recorded during a previous study (Manis, 1990) but were not discussed in that report. One of the Lucifer yellow-stained simple spiking cells from that study was reacted with an antibody to Lucifer yellow to permit a more detailed morphological analysis for the present study; the other simple spiking cells were recorded during the present experiments.

Physiology of complex spiking neurons

The complex action potential consisted of an initial fast action potential followed within 10 msec by one or more lower amplitude fast action potential(s) riding on a slow depolarization followed by a long after-hyperpolarization (Fig. 1). In most cells, the bursts occurred in an all-or-none fashion whether appearing as spontaneous or evoked discharges. However, in three of 29 cells, both bursts and isolated single spikes were seen. When they occurred, single spikes were followed by an after-depolarization–after-hyperpolarization sequence that was distinct from the characteristic two-component after-hyperpolarizations seen in many simple spiking cells. Most of the complex spiking cells were spontaneously active in the absence of any holding current, so subsequent physiological characterization of the cells was performed with sufficient holding current to stop the spontaneous discharges. Three cells required no holding current, 15 required less than −200 pA, and 11 required between −200 and −1,000 pA.

Typical responses to depolarizing current pulses delivered from rest are shown in Figure 2A (this cell had no spontaneous activity). Small current pulses (< 0.2 nA) give rise to one or two isolated bursts. The membrane potential slowly depolarizes during the current pulse before reaching the threshold for the burst. Large pulses result in a regular train of bursts, although, after the first burst, the response usually consists of a single fast action potential riding on a slow depolarization that is followed by a large after-depolarization. Trains of bursts occur at a rate of 20–60 Hz. Following the current pulses, particularly for pulses > 0.5 nA, there is a prolonged hyperpolarization. The duration of this after-hyperpolarization is longer in complex spiking neurons than in simple spiking cells.

The responses to small hyperpolarizing current pulses (< −0.4 nA) are characterized by approximately exponential charging trajectories (Fig. 2A, −0.9 nA), with a mean time constant for −0.2 nA pulses of 9.4 ± 5.3 msec. For larger current steps, a voltage sag becomes evident (Fig. 2A, solid arrowhead; −0.9 nA). A large anodal break response is characteristic of the complex spiking cells (Fig. 2C, arrow). This potential is often large enough to bring the cell to threshold for a complex spike burst, particularly for large current steps.

Current-voltage relationships at two times during the current pulse are illustrated in Figure 2B for one representative complex spiking cell. At early times (squares, 15–25

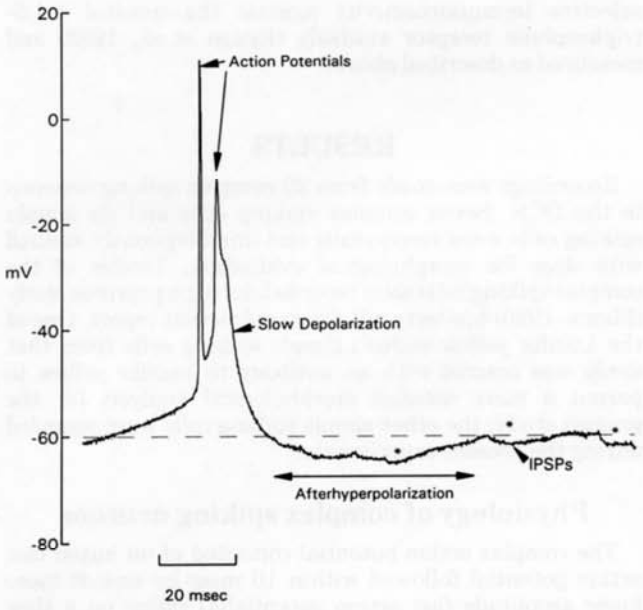

Fig. 1. Configuration of the spike burst. The complex spike burst consists of a volley of fast action potentials (in this case 2) of decreasing amplitude and separated by 2–10 msec. The action potentials ride on a slow depolarization. The burst is followed by a prolonged hyperpolarization. This trace also shows spontaneous inhibitory postsynaptic potentials (IPSPs; indicated by asterisks) during the after-hyperpolarization. Cell: 13OCT89C.

msec after step, corresponding to the maximum voltage change), the current-voltage relationship is approximately linear for small depolarizing and most hyperpolarizing current injections. At later times (circles, 95 msec after the beginning of the 100 msec step), most cells exhibit a time and voltage-dependent sag during hyperpolarizing current steps, as indicated by the deviation between the curves at the two different times for larger hyperpolarizing current steps. The sag in voltage appears as early as 15 msec into the current injection. The sag appears to have a threshold for activation 10–20 mV below rest, and is evident to some extent in 12 of 21 complex spiking cells for which responses to −1.0 nA current pulses were collected. An additional time-dependent rectification is evident for small depolarizing pulses (<0.1 nA) when the current-voltage relationship is determined late during the current pulse (indicated by arrowhead in Fig. 2B). This rectification appears for membrane potentials just above rest and often can bring the cell to threshold for burst generation during the current pulse, even for pulses of approximately 0.1 nA.

The *burst* discharge rate (i.e., the rate of slow depolarizations) was determined as a function of injection current. The burst discharge rate increased approximately linearly up to 0.5 nA (Fig. 2D; data shown are for four different cells), then saturated at 40–80 Hz for larger currents. If individual fast action potentials were counted, the discharge rate would exhibit a steep initial slope but would saturate at two to four times the bursting rate above 0.5 nA because two to four identifiable fast action potentials occur during each burst. Frequently, only an initial action potential could be clearly identified in the burst responses with large current pulses. In these cases, the initial fast action potential is followed by a slow depolarization without additional identifiable action potentials (see, e.g., Fig. 2A; 0.7 nA).

Simple spikes were evident in the spontaneous and driven discharge of three of 29 complex spiking neurons. Traces 1 and 2 in Figure 3A show the spontaneous activity of one complex spiking cell that alternated between simple spiking and complex spiking modes several times a minute. Both the complex and simple spikes occurred at regular intervals. The simple spikes differ from those of identified pyramidal cells (Manis, 1990) in that they show a distinct after-depolarization (indicated by the triangles) that separates the rapid downstroke of the spike and a slow after-hyperpolarization. Figure 3B, traces 1 and 2, shows the discharge of two other cells in response to a small depolarizing current pulse. The cells discharged both isolated action potentials with an after-depolarization (indicated by triangles) and complex spikes. Although these observations were fairly rare in our sample, they suggest that these cells may have more than one mode of discharge.

The complex spiking cells also frequently exhibited spontaneous IPSPs, as marked by asterisks in the traces of Figures 1 and 2A. These IPSPs occurred with a high rate and sometimes appeared as bursts of two to three events that summated to produce a larger IPSP (Fig. 2A).

The amplitude of the fast action potentials within a burst was graded. Action potential amplitudes are plotted in Figure 4A as a function of the previous interspike interval for data from one typical complex spiking cell. Spike amplitudes were measured from discharges occurring spontaneously and from discharges resulting from small depolarizing current pulses. The spike amplitude decreases rapidly for interspike intervals less than about 5 msec (Fig. 4A), corresponding to spikes produced subsequent to the first spike within a burst (first spikes are indicated by solid circles, second spikes by open squares, and third spikes by solid triangles). The inset shows the interspike interval distribution for this cell; spikes preceded by an interval greater than 15 msec (marked by arrow) were the first spikes of a burst. The remainder of the spikes occurred within bursts and were preceded by an interval less than 6 msec. The changes in spike amplitude (and shape) that occur within a burst are probably due to accumulated inactivation of sodium channels during the spike burst because the membrane potential between spikes is much less negative than between bursts. This idea is supported by the analysis shown in Figure 4B. Here, it is evident that the amplitude of a secondary or tertiary spike within a burst is highly correlated with the minimum potential seen between that spike and the preceding spike. The secondary and tertiary spikes also have smaller rising and falling slopes (Fig. 4C,D) and broader half-widths (not shown). These measures all suggest that the properties of the first spike and the subsequent spikes in a burst form a continuum.

The electrical properties of complex spiking cells are summarized in Table 1. In comparison to a previous analysis of simple spiking cells of the DCN from the same laboratory (Manis, 1990), only two parameters were significantly ($P < 0.05$, two-tailed t-test) different. The first spike within a burst in complex spiking cells was asymmetrical compared to first spikes of simple spiking cells, in that the spike had a larger ratio between the rising and falling slopes. The first action potential of the burst in the complex spiking cells was also wider than the individual action potentials of simple spiking cells, in part because of the

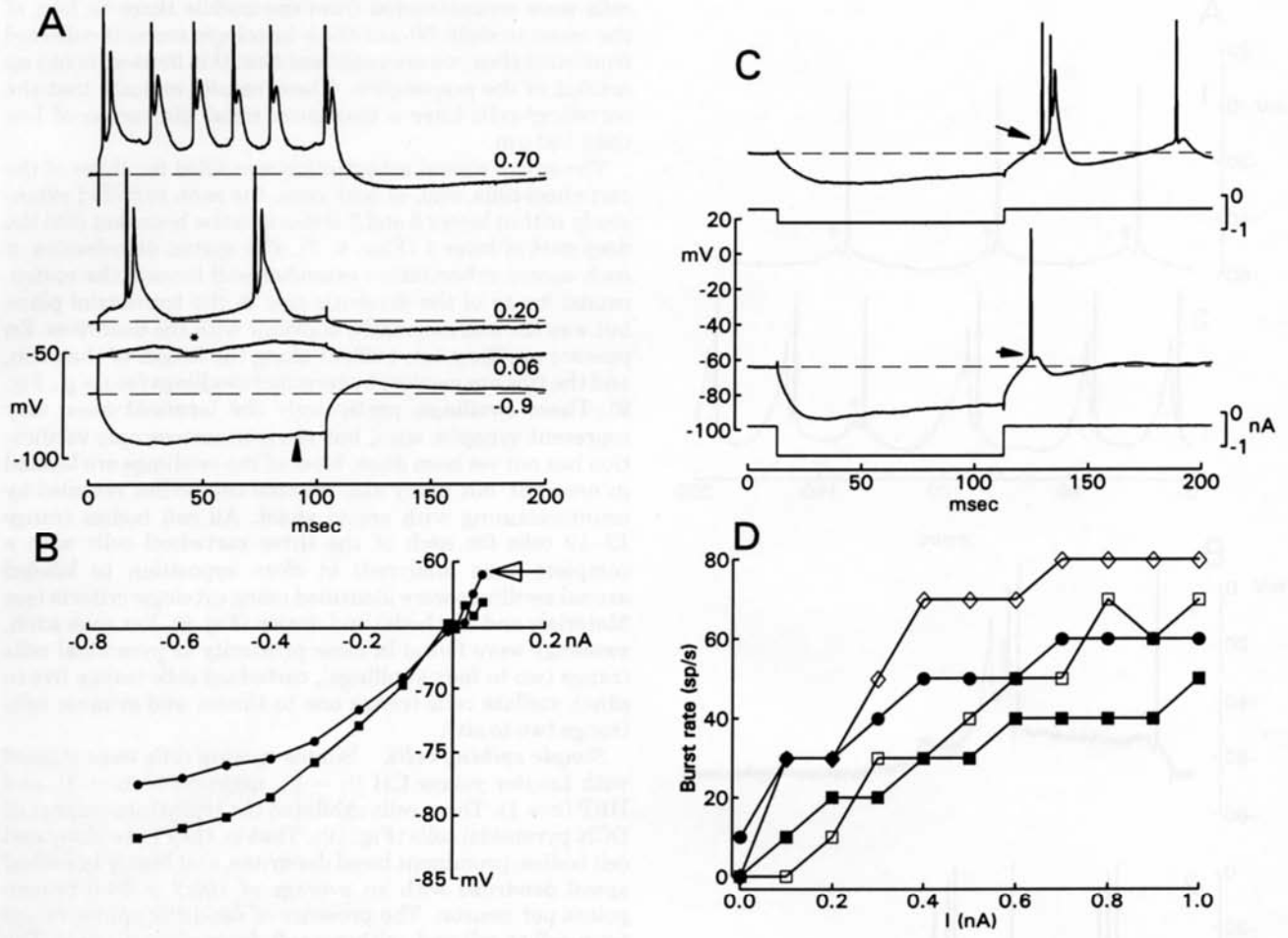

Fig. 2. Responses of a complex spiking neuron to short current pulses. **A:** Responses of a complex spiking cell to depolarizing and hyperpolarizing current pulses. The membrane potential shows an exponential charging trajectory in response to hyperpolarizing current pulses, sometimes followed by a slight sag (evident in −0.9 nA trace, arrowhead). Subthreshold depolarizations (0.06 nA) produce a slowly rising response, in this case punctuated by a train of IPSPs, marked by an asterisk. Depolarizing pulses produce either isolated bursts (0.2 nA) or trains of bursts (0.7 nA). A prolonged hyperpolarization follows the burst or burst train. **B:** Subthreshold current-voltage relationships for complex spiking cell. Squares mark the current-voltage relationship measured at 15–35 msec into the current pulse; circles mark the relationship at 95 msec after the start of the current pulse. The upward deviation present for the late measurement of hyperpolarizing responses corresponds to an inward or anomalous rectification. For small depolarizing pulses, there is a weak inward rectification, as indicated by the upward turn of the curves for positive current (marked by open arrow). **C:** Complex spiking cells fire anodal break bursts. Two traces from one cell illustrating a burst (arrow, top trace) and a simple spike (arrowhead, lower trace) evoked following hyperpolarizing current steps of different amplitudes. **D:** Burst discharge rate vs. current injection relationship. Results from four individual cells are superimposed. The discharge rate shows some saturation above 0.5 nA, with a maximal rate for different cells between 40 and 80 Hz. A,B: cell 13OCT89C; C: cell 29DEC92K.

slower falling slope of the action potential in the complex spiking cells.

Morphology

Seven complex spiking cells and six simple spiking cells were unambiguously recovered following histologic processing of the tissue slices. The peroxidase-DAB reaction product obscured internal cytological features of the stained cells, but other morphologic characteristics revealed a somatic grouping consistent with the two distinct spiking classes (Fig. 5). The complex spiking cells exhibited cell bodies located in the deep part of layer 1 or the superficial part of layer 2. Their oval somata had dimensions (open circles, Fig. 5) whose values clustered within those of the population of cartwheel cells identified by IP_3 receptor immunostaining (Ryugo et al., 1992; indicated by plus signs in Fig. 5). In contrast, the stained simple spiking cells (solid circles, Fig. 5) were located in the middle of layer 2 and had an elongate shape whose somatic dimensions were distributed with those of pyramidal cells identified on the basis of their appearance in Nissl-stained sections from slices (multiplication signs Fig. 5; see also Table 2).

Complex spiking cells. Complex spiking cells were stained with Lucifer yellow CH (n = 2), neurocytin (n = 3), and HRP (n = 2). All stained cells were recorded in slices cut in the transstrial plane. The dendritic morphology of these neurons was consistent with the previously established criteria for cartwheel cells in the guinea pig (Hackney

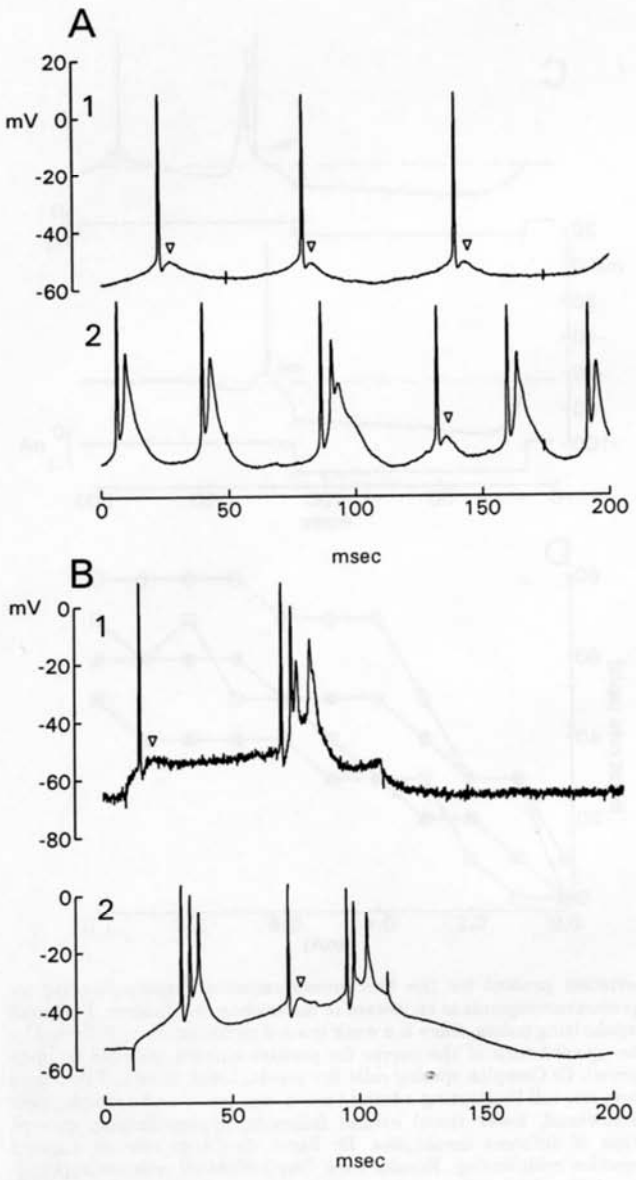

Fig. 3. Simple spikes and bursts can occur together. **A:** Traces 1 and 2 show portions of an alternation between simple and complex spiking patterns recorded from one cell. Note that, when the cell does not burst, the spikes are followed by a distinct after-depolarization (indicated by inverted triangles). Cell 13JUN89C. **B:** Traces 1 and 2 show mixed firing modes in response to depolarizing current pulses in two other cells in which both simple and complex spikes were produced. Cells 5APR91B and 2SEP88C.

et al., 1990; Berrebi and Mugnaini, 1991). There are no basal dendrites, and the spiny, apical dendrites extend into the molecular layer (Figs. 6, 7). The range of primary dendrites per cell was three to six, with an average of 4.3 ± 1.4. These dendrites branch rather infrequently, exhibiting an average of 27 ± 4.5 branch points per neuron. Along their length, the dendrites are constant in diameter and studded with small, short spines (Fig. 8A). At their tips, the dendrites taper abruptly yet remain spiny (Fig. 8B).

The dendritic domains of each of these cells appears to be flattened within the transstrial plane. Because all recovered cells were reconstructed from the middle three to four of the seven to eight 50-μm-thick histologic sections collected from each slice, we are confident that this flatness is not an artifact of the preparation. These results indicate that the cartwheel cells have a maximum strial dimension of less than 150 μm.

The entire axonal arborization was filled for three of the cartwheel cells, and, in each case, the axon ramified extensively within layers 2 and 3 and sent a few branches into the deep part of layer 1 (Figs. 6, 7). The spatial distribution of each axonal arborization extended well beyond the rostrocaudal limits of the dendritic tree in the transstrial plane but was flat and essentially coplanar with the dendrites. En passant swellings are evident along the length of the axon, and the tips are marked by terminal swellings (see, e.g., Fig. 9). These swellings, particularly the terminal ones, may represent synaptic sites, but electron microscopic verification has not yet been done. Most of the swellings are located in neuropil, but many also abutted cell bodies revealed by counterstaining with cresyl violet. All cell bodies (range 12–19 cells for each of the three cartwheel cells with a complete axon analyzed) in close apposition to labeled axonal swellings were identified using cytologic criteria (see Materials and Methods) and drawn (Fig. 9). For each axon, swellings were found in close proximity to pyramidal cells (range two to four swellings), cartwheel cells (range five to nine), stellate cells (range one to three), and granule cells (range two to six).

Simple spiking cells. Simple spiking cells were stained with Lucifer yellow CH (n = 2), neurocytin (n = 3), and HRP (n = 1). These cells exhibited the typical appearance of DCN pyramidal cells (Fig. 10). That is, they have elongated cell bodies, prominent basal dendrites, and highly branched apical dendrites with an average of 190.2 ± 64.5 branch points per neuron. The presence of dendritic spines varied from cell to cell and, within a cell, from place to place. The basal dendrites were typically smooth, although one cell exhibited frequent spines along its main shafts (Fig. 8C), with fewer spines toward their terminations. The shafts of apical dendrites were smooth (Fig. 8D), but the terminal dendritic branches tended to be more variable in appearance. One characteristic feature along the dendritic shaft was the presence of short branches, some resembling long dendritic spines and others being irregularly varicose (Fig. 8E). These terminal branches were usually marked by an angular swelling at their tips (Fig. 8F,G). One cell also exhibited numerous spines along these terminal branches (Fig. 8H). Axons were not recovered for any of the simple spiking cells.

DISCUSSION

Identity of recorded cells

The electrical properties of neurons recorded from the dorsal cochlear nucleus in the slice preparation fall into two categories: simple spiking and complex spiking cells. Simple spiking cells have been identified as pyramidal cells, tuberculoventral cells, molecular layer stellate cells, and giant cells (Rhode et al., 1983; Smith and Rhode, 1985; Oertel and Wu, 1989; Manis, 1990; Zhang and Oertel, 1993b,c). Oertel and Wu (1989) also reported two cartwheel cells with simple spikes, but see discussion in Zhang and Oertel

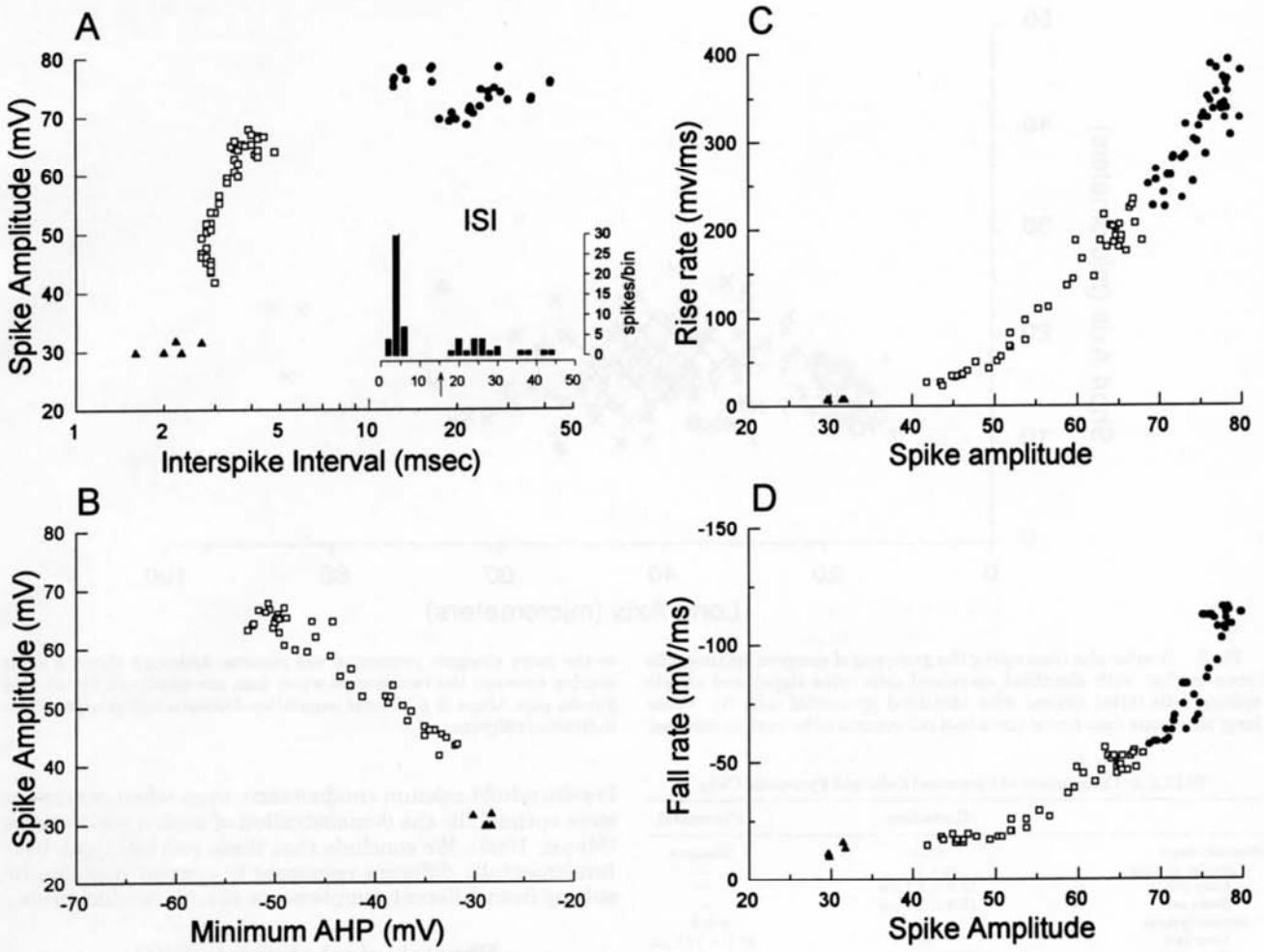

Fig. 4. Spike amplitude and shape depend on the interspike interval (ISI) and the order of a spike within a burst. For all panels, the solid circles represent measurements made from the first spike within a burst; open squares are measurements from secondary spikes, and solid triangles are from tertiary spikes within a burst. **A:** Spike amplitude decreases with interspike intervals less than 5 msec. Spikes with previous interspike intervals greater than 50 msec are not plotted. **Inset:** Interspike interval distribution for all spikes in this figure. The interspike interval distribution is bimodal. Spikes with preceding intervals greater than 15 msec (indicated by arrow) are the first spike within a burst. Subsequent spikes within the burst occur at intervals of less than 6 msec. **B:** The amplitude of secondary and tertiary spikes is inversely related to the amplitude of the prior after-hyperpolarization (AHP). Minimum AHP was measured as the minimum absolute voltage that occurred between the first and second spikes or between the second and third spikes. Spike number within each burst coded as in A. **C:** Maximum rising rate of voltage change (dv/dt, in mV/ms) is larger for spikes of larger height, and is largest among first spikes. **D:** Maximum falling rate of spike (in mV/msec) is larger for spikes of larger amplitude and is largest among first spikes. Cell 3NOV88A.

(1993b, p. 1,395). In contrast, complex spiking cells are small, superficial neurons that emit spiny apical dendrites into the molecular layer and have no basal dendrites. Cells with this morphology have been identified as cartwheel neurons (Lorente de Nó, 1933, 1981; Brawer et al., 1974; Kane, 1974; Wouterlood and Mugnaini, 1984; Hackney et al., 1990; Berrebi and Mugnaini, 1991).

Because complex spiking cells are small, one concern is that some of their properties may be either caused by or altered by damage to the cell from the recording electrode. Four lines of evidence suggest that damage, per se, is not responsible for the complex spiking pattern. First, in some cells, such spiking patterns could be recorded for periods of up to 90 minutes, and, during this time, the discharge properties of the cells did not change. Complex spiking cells

TABLE 1. Electrical Characteristics of Complex Spiking Neurons[1]

Measure	Value	N
V_m (mV)	−57.9 ± 17.7	27
R_{in} (MΩ)	31.1 ± 21.9	24
τ (msec)	9.4 ± 5.3	23
First spike height (mV)	64.6 ± 11.6	20
Spike half-width (msec)	1.012 ± 0.504	20
Rise dv/dt (mV/msec)	230 ± 65	20
Fall dv/dt (mV/msec)	94 ± 27	20
Rise/fall	2.59 ± 0.64	20

[1]Cells included for analysis only if spike height >50 mV. The primary charging time constant (τ) was obtained from a simplex curve fit of an exponential function to the transient decay phase (excluding the first 1.0–1.5 msec) of the response to hyperpolarizing current pulses of −0.2 to −0.4 nA. Input resistances (R_{in}) were calculated from the slope of current-voltage relationship just below rest, determined at the end of a 100 msec pulse. Spike parameters were measured for the first spike within a burst for spontaneous bursts or responses to small (<0.2 nA) current pulses. Spike heights are measured from baseline; rising and falling slopes are maximal slope values determined over the interval occupied by the spike. Values are given as mean ± standard deviation.

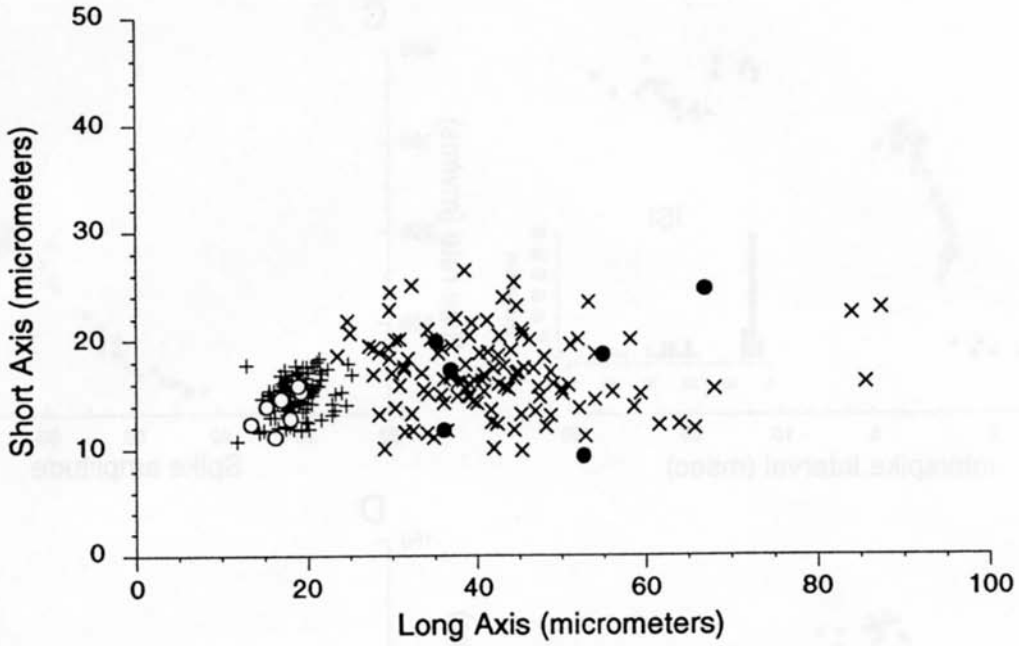

Fig 5. Scatter plot illustrating the grouping of complex spiking cells (open circles) with identified cartwheel cells (plus signs) and simple spiking cells (filled circles) with identified pyramidal cells (x). These long/short axis data reveal cartwheel cell somata to be oval, in contrast to the more elongate pyramidal cell somata. Although there is some overlap between the two groups when data are combined for all nine guinea pigs, there is a distinct separation between cell groups within individual subjects.

TABLE 2. Comparison of Cartwheel Cells and Pyramidal Cells

	Cartwheel	Pyramidal
Somatic shape	Oval	Elongate
Complex spiking	n = 7	—
Long axis	16.8 ± 2.1 μm	—
Short axis	13.8 ± 1.7 μm	—
Simple spiking	—	n = 6
Long axis	—	47.1 ± 13.0 μm
Short axis	—	17.0 ± 5.6 μm
Cytologic identity	n = 138	n = 117
Long axis	18.5 ± 2.2 μm	42.1 ± 11.5 μm
Short axis	15.0 ± 1.6 μm	17.0 ± 3.6 μm
Basal dendrites	No	Yes
Apical dendrites	Yes	Yes
Primary dendrites	4.3 ± 1.7	4.4 ± 1.1
Branch points	27.0 ± 4.5	190 ± 14.5
Spines	High density	Variable
Shafts	Spiny	No spines
Terminal branches	Spiny	Some spines

never became simple spiking cells (and vice versa), even when their responses deteriorated during the recording session. Second, cells with spike doublets and triplets can be recorded extracellularly in the slice (Manis, unpublished observations; Waller and Godfrey, 1994) and in vivo (Spirou et al., 1993; Table 1), suggesting that such discharge patterns are not necessarily the consequence of a damaging electrode penetration into the cell. Third, simple and complex spiking cells can be differentiated according to their responses to changes in extracellular potassium or calcium or the application of adenosine, muscarine, and barium (Waller and Godfrey, 1991; Chen et al., 1993; Waller and Godfrey, 1994). Fourth, most complex spiking cells exhibit pronounced anodal rebound responses, such as would be generated by a low-threshold calcium conductance (Llinás and Yarom, 1981; Carbone and Lux, 1984, Fox et al., 1987). In contrast, simple spiking cells never exhibited such a strong rebound response or any evidence for a low-threshold calcium conductance, even when conditions were optimal for the demonstration of such a conductance (Manis, 1990). We conclude that these two cell types have fundamentally different responses to current injection resulting from different complements of ionic conductances.

Physiological characteristics of cartwheel neurons

The cartwheel cells are in many ways analogous to the cerebellar Purkinje cell (Mugnaini and Morgan, 1987; Berrebi and Mugnaini, 1991), so it is useful to compare the membrane characteristics of Purkinje cells and cartwheel cells. Both neuronal types discharge complex action potential bursts in response to depolarizing current (Purkinje cells, Llinas and Sugimori, 1980; cartwheel cells, Zhang and Oertel, 1993a; present study), exhibit anomalous rectification for hyperpolarizing steps (Purkinje cells, Crepel and Penit-Soria, 1986; cartwheel cells, present study), and show inward rectification for small depolarizing steps from rest (Purkinje cells, Llinas and Sugimori, 1980; cartwheel cells, Hirsch and Oertel, 1988; present study).

However, several characteristics of the cells are quite distinct. First, Purkinje cells fire simple spikes without strong after-depolarizations during injection of small currents, whereas guinea pig cartwheel cells usually discharge complex spikes at all current injection levels. When simple spikes are seen in complex spiking cells, they are followed by a characteristic after-depolarization (see, e.g., Figs. 2C, bottom, and 3A). Second, Purkinje cells fire complex spikes followed by a plateau potential for large current injections. In contrast, plateau responses were seen rarely seen (one of 29 cells) in the present study. Third, mature Purkinje cells do not fire anodal break bursts, whereas such bursts are frequently seen in cartwheel neurons. It should be noted

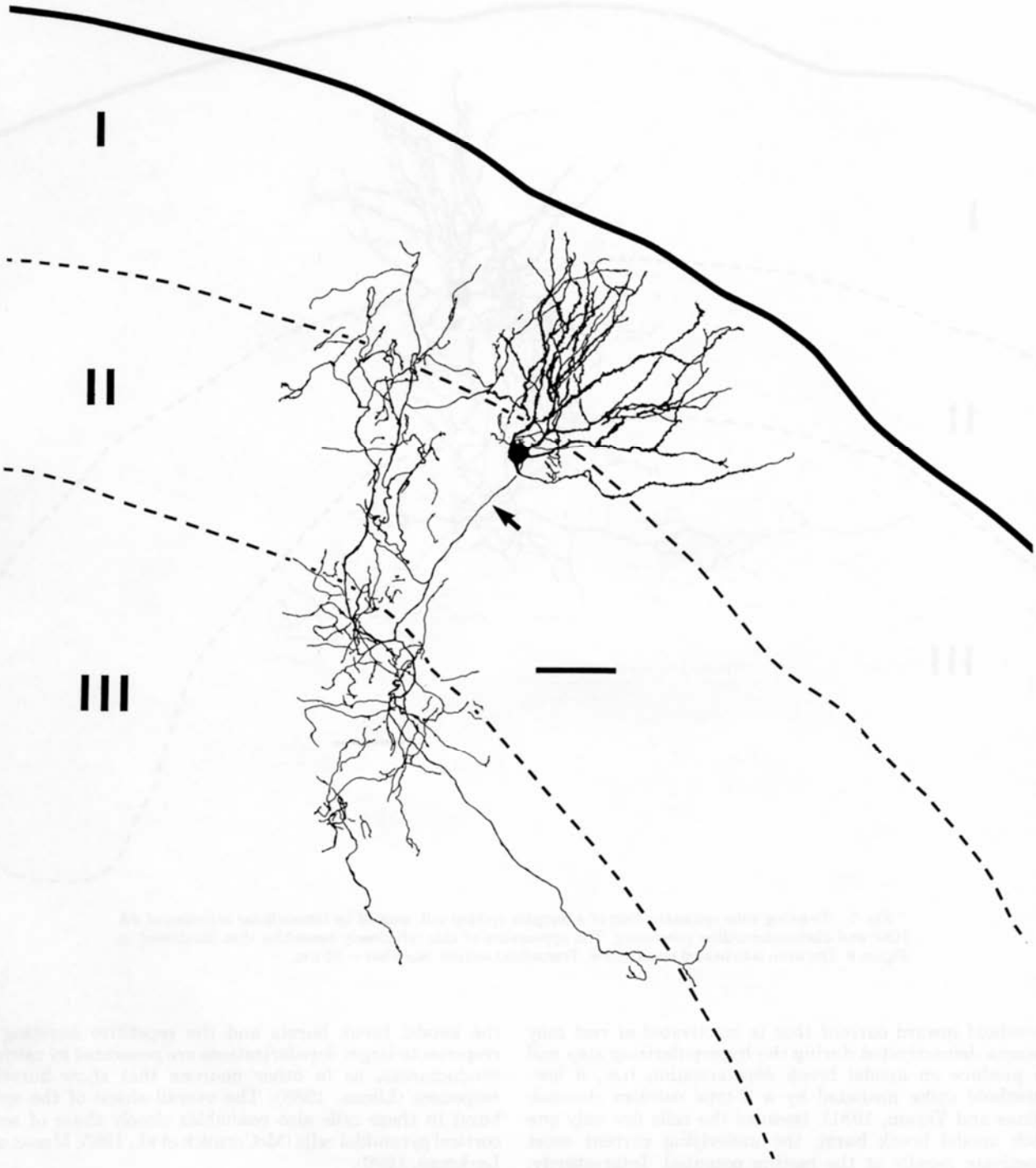

Fig. 6. Drawing tube reconstruction of a complex spiking cell stained by intracellular injection of 4% neurocytin followed by avidin-biotin and diaminobenzidine processing. The spiny dendrites are relatively unbranched, whereas the axon (arrow) is highly ramified within layers I, II, and III. The pial surface is toward the upper right, indicated by the solid line. Transstrial section. Scale bar = 50 μm.

that, in our recordings, few cells fired action potentials that were not associated with an underlying burst depolarization, whereas the complex spiking cells recorded from mouse brain slices by Hirsch and Oertel (1988) and Zhang and Oertel (1993a) did show such simple spiking activity in conjunction with bursts. In addition, the cartwheel cells from mouse did not exhibit anodal break bursts (Zhang and Oertel, 1993a), whereas this was a common feature of the guinea pig cells.

The complex action potentials in cartwheel neurons may be initiated by two different mechanisms. First, bursts are readily generated at the end of a hyperpolarizing current step, when the cell nominally is returned to the resting potential. This response pattern suggests that a low-

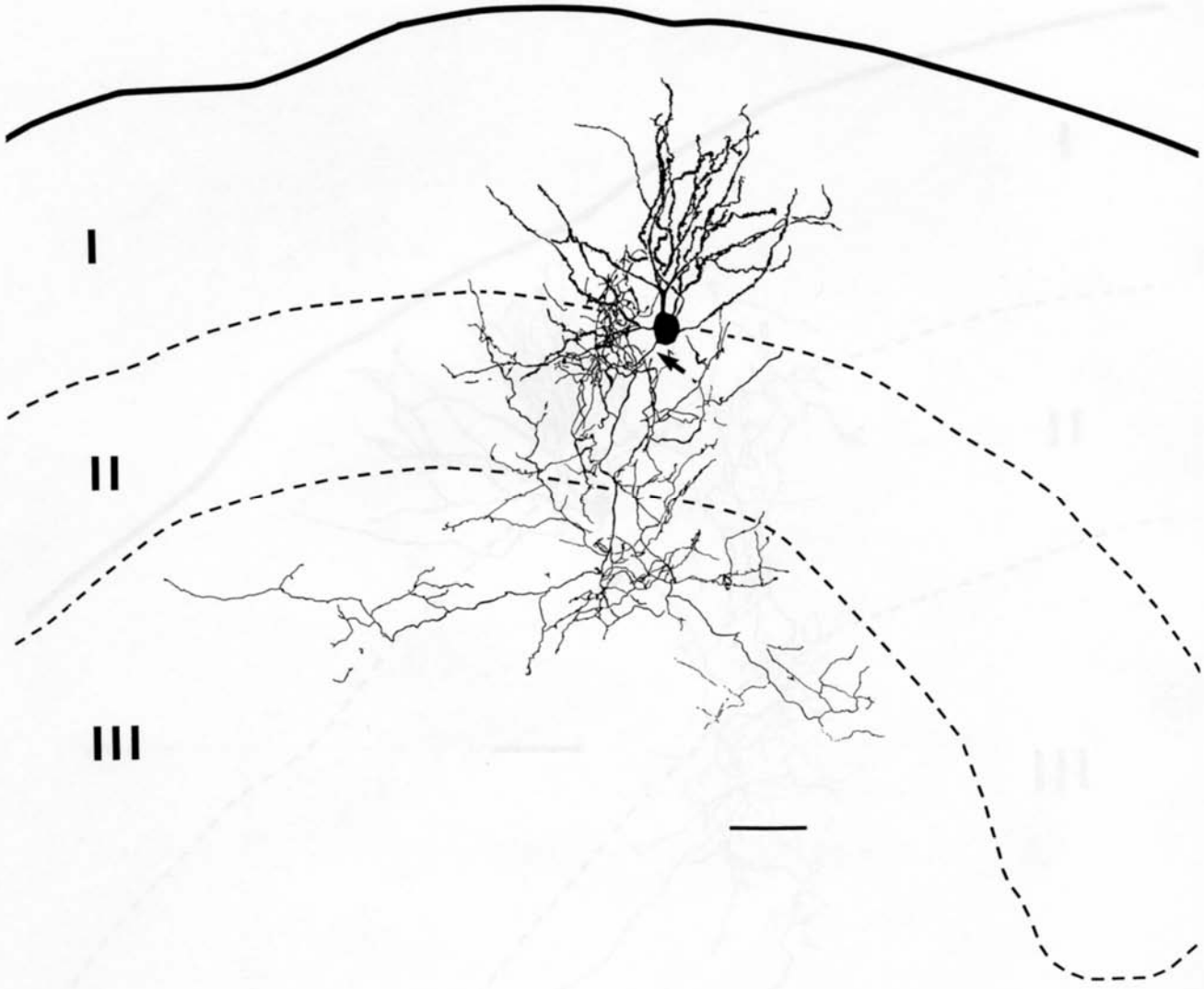

Fig. 7. Drawing tube reconstruction of a complex spiking cell, stained by intracellular injection of 4% HRP and diaminobenzidine processing. The appearance of this cell closely resembles that illustrated in Figure 6. The axon is indicated by an arrow. Transstrial section. Scale bar = 50 μm.

threshold inward current that is inactivated at rest may become deinactivated during the hyperpolarizing step and so produce an anodal break depolarization (i.e., a low-threshold spike mediated by a T-type calcium channel; Llinas and Yarom, 1981). Because the cells fire only one such anodal break burst, the underlying current must inactivate rapidly at the resting potential. Interestingly, low-threshold calcium currents and anodal break bursts appear to be weak or absent in adult Purkinje cells (Llinas and Sugimori, 1980; but see Crepel and Penit-Soria, 1986). Second, additional conductances with higher thresholds are apparently present because the trains of bursts are produced by depolarizing current injections. These bursts occur at membrane potentials where a low-threshold conductance should be inactivated and, therefore, are most likely produced by high-voltage noninactivating calcium channels of the L, N, or P types (Fox et al., 1987; Regan, 1991). Support for the involvement of calcium conductances in the generation of bursting responses in the DCN has been presented by Hirsch and Oertel (1988); it is likely that both the anodal break bursts and the repetitive bursting in response to larger depolarizations are generated by calcium conductances, as in other neurons that show bursting responses (Llinas, 1988). The overall shape of the spike burst in these cells also resembles closely those of some cortical pyramidal cells (McCormick et al., 1985; Mason and Larkman, 1990).

The presence of these complex bursts, and their putative (but likely) generation by calcium conductances, suggests that the cellular calcium levels will be highly correlated with the electrical activity of the cell. The existence in cartwheel neurons of calcium binding proteins (e.g., PEP-19; Berrebi and Mugnaini, 1991) as well as IP_3 receptors (Mignery et al., 1989; Ryugo et al., 1992) that presumably regulate release of calcium from intracellular stores suggests that control of the intracellular calcium level in these cells is important to their function. However, the role that intracellular calcium plays in regulating the activity or modulating the membrane function of these cells is presently not known.

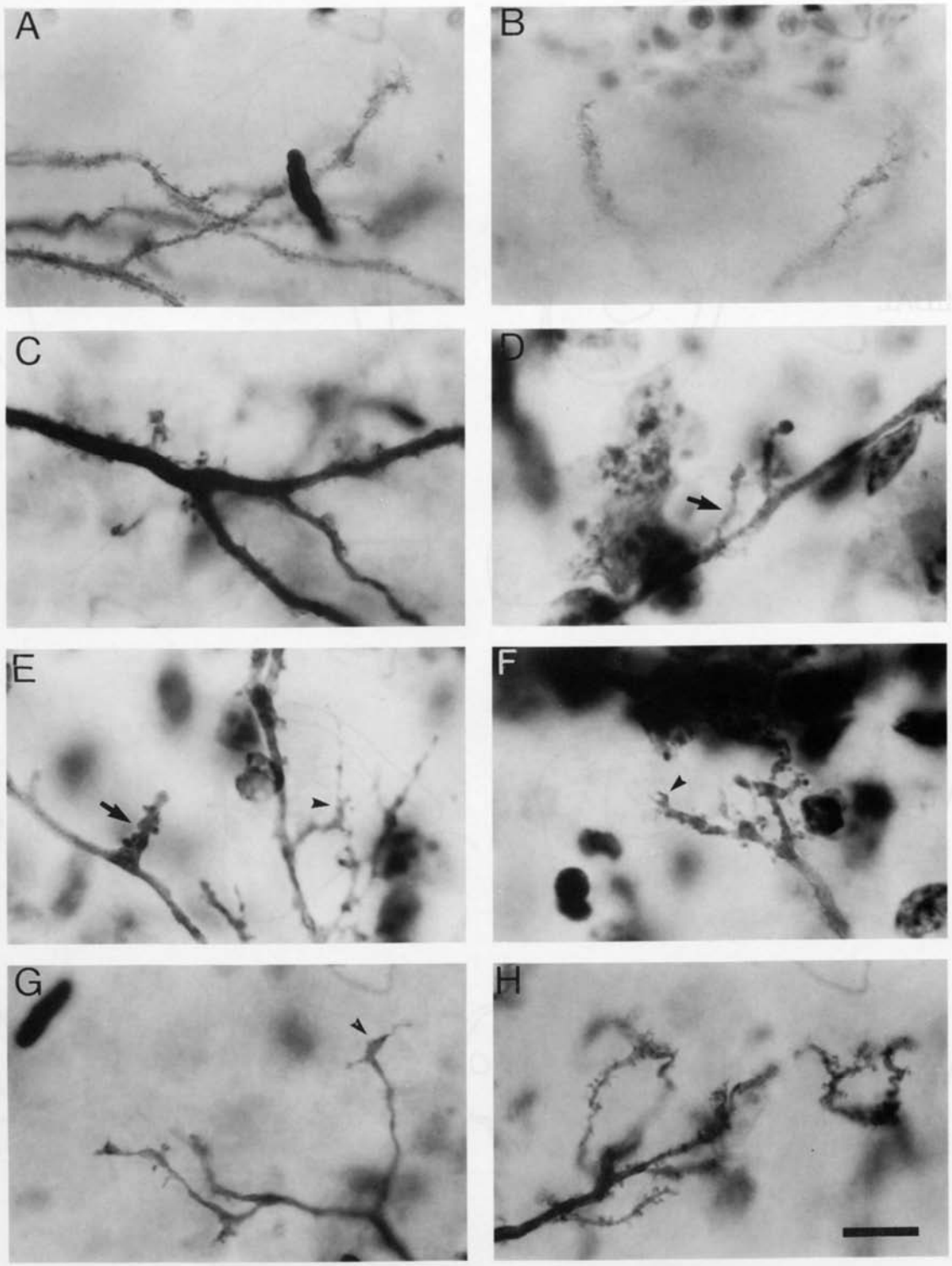

Fig. 8. Photomicrographs illustrating key features of labeled dendrites. **A:** The dendritic shafts of cartwheel cells are always laden with spines. **B:** The tips of cartwheel cell dendrites taper to a sharp point and are also spiny. **C:** The basal dendritic shafts of pyramidal cells are typically without spines, but one particular cell exhibited some spines. **D:** Apical dendritic shafts of pyramidal cells are devoid of spines. **D,E:** Short dendritic branches (arrow) commonly arise from shafts of pyramidal cells; **E–G:** The tips of the apical dendrites of pyramidal cells are marked by irregular swellings, from which hair-like appendages often emanate (arrowheads). **H:** Spiny terminal dendrites, although rare, are shown from the same pyramidal cell illustrated in C. Scale bar = 10 μm.

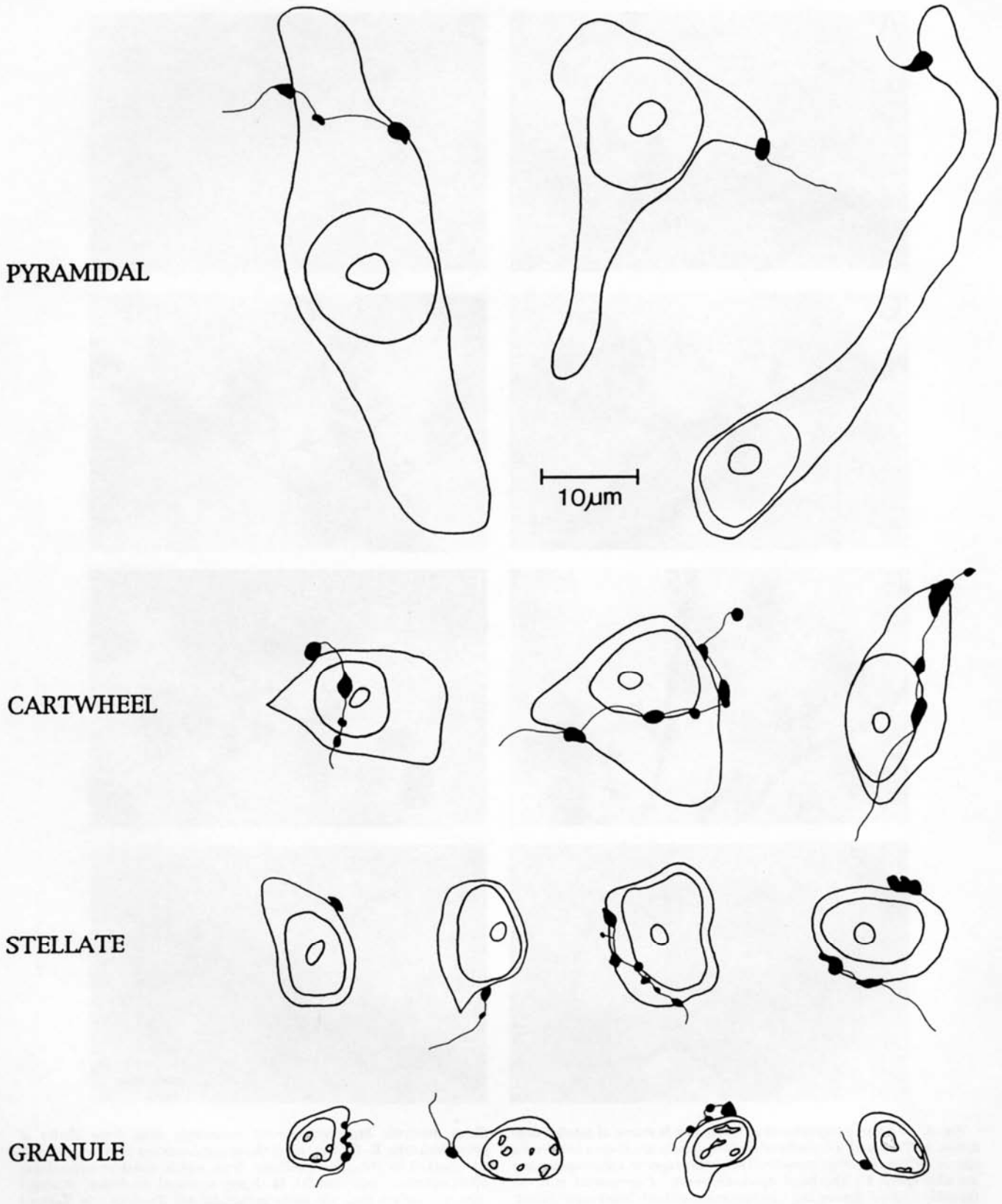

Fig. 9. Drawing tube reconstruction of cresyl violet stained somata in apposition with labeled axonal swellings of cartwheel cells. The three recovered axons all exhibited swellings associated with these four classes of cells.

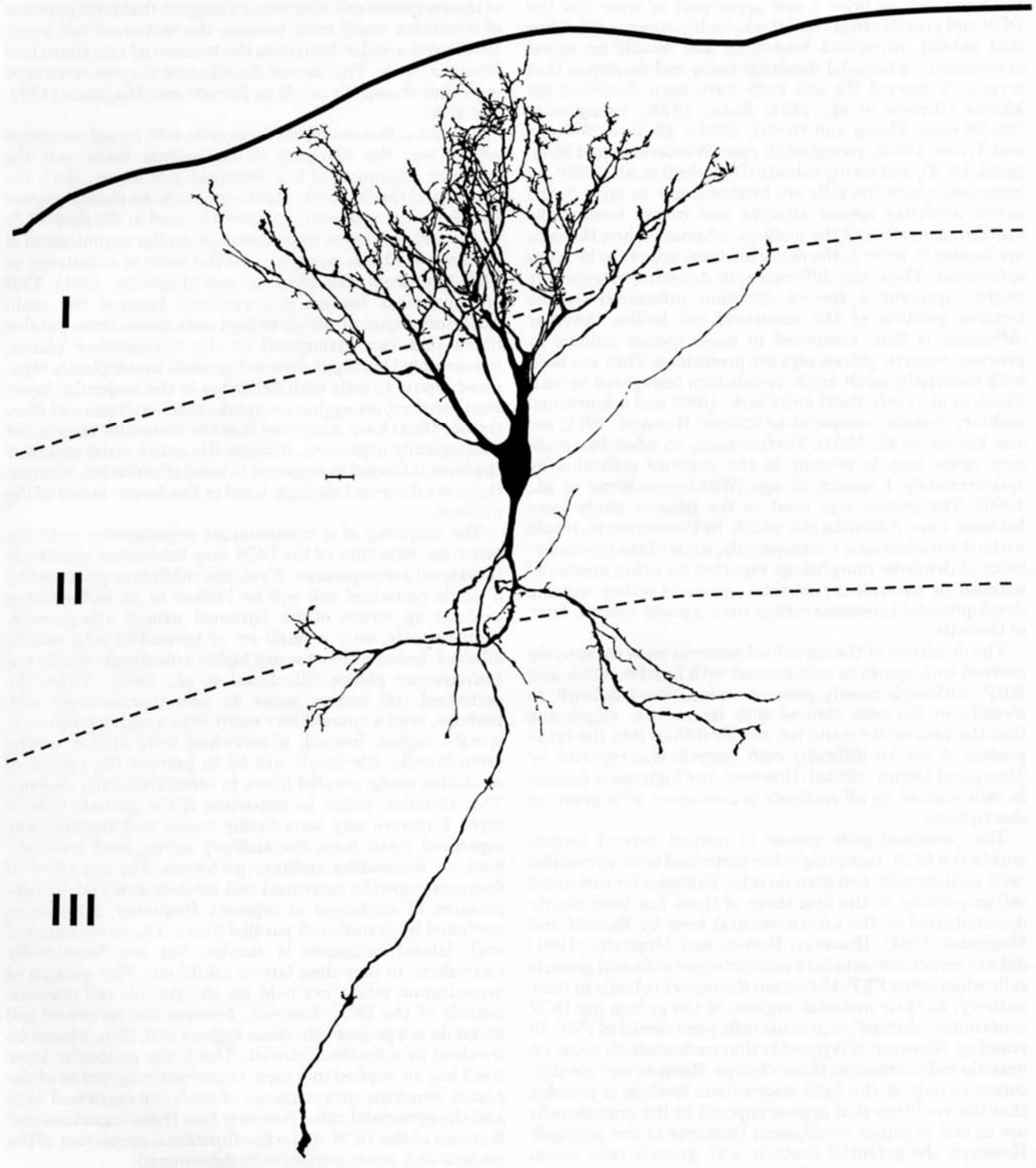

Fig. 10. Drawing tube reconstruction of a simple spiking cell stained by intracellular injection of 4% Lucifer yellow. Tissue was processed using anti-Lucifer yellow, biotinylated secondary antibody, avidin-biotin, and diaminobenzidine. All recovered simple spiking cells exhibit the classic appearance of pyramidal neurons. Transstrial section. Scale bar = 20 μm.

Morphology of cartwheel neurons

The morphology of complex spiking cells that were stained by intracellular injections and histologically recovered in the present study matched the descriptions of cartwheel cells (also called globular cells by Lorente de Nó, 1981), as revealed by Golgi staining methods in young adult guinea pigs (Hackney at al., 1990) and in some young cats (Lorente de Nó, 1981, Figs. 6–12). The cell bodies reside in

the lower part of layer 1 and upper part of layer 2 of the DCN and give rise to several thick, highly spinous dendrites that exhibit infrequent branching and mostly an apical orientation. Spheroidal dendritic fields and dendrites that turn back toward the cell body have been described for kittens (Brawer et al., 1974; Kane, 1974), young mice (20–29 days, Zhang and Oertel, 1993a; 45 days, Webster and Trune, 1982), young adult rats (Wouterlood and Mugnaini, 1984), and young rabbits (Disterhoft et al., 1980). In instances where the cells are located closer to layer 2, the apical dendrites appear straight and course toward the ependymal surface of the nucleus, whereas, when the cells are located in layer 1, the dendritic trees appear to be more spheriodal. Thus, the differences in dendritic morphology might represent a species variation influenced by the laminar position of the cartwheel cell bodies. Another difference is that, compared to most species studied in previous reports, guinea pigs are precocious. They are born with essentially adult brain metabolism (compared to rats; Booth et al., 1980; Patel and Clark, 1980) and a functional auditory system (compared to kittens; Romand, 1971; see also Horner et al., 1987). Furthermore, an adult-like auditory space map is present in the superior colliculus by approximately 1 month of age (Withington-Wray et al., 1990). The guinea pigs used in the present study were between 1 and 3 months old, which, by these criteria, would make them adult-like. Consequently, some of the characteristics of dendritic morphology reported for other species of younger or equivalent postnatal age could reflect ongoing developmental processes rather than a more mature form of the cells.

The dendrites of the cartwheel neurons were extensively covered with spines in cells stained with Lucifer yellow and HRP. Although clearly present, spines were difficult to identify in the cells stained with neurocytin, suggesting that the neurocytin could not readily diffuse into the spine process. A similar difficulty with biocytin was reported by Zhang and Oertel (1993a). However, the high spine density in cells stained by all methods is consistent with previous descriptions.

The cartwheel cells appear to contact several targets within the DCN, including other cartwheel cells, pyramidal cells, stellate cells, and granule cells. Evidence for cartwheel cell projections to the first three of these has been clearly demonstrated at the ultrastructural level by Berrebi and Mugnaini (1991). However, Berrebi and Mugnaini (1991) did not report contacts between cartwheel cells and granule cells when using PEP-19 to stain the cartwheel cells in their entirety. In their material, regions of the guinea pig DCN containing "clumps" of granule cells were devoid of PEP-19 staining. However, it is possible that such contacts occur on granule cells outside of these clumps. Because our identification is only at the light microscopic level, it is possible that the swellings that appear apposed to the granule cells are in fact synapses on adjacent elements in the neuropil. However, the potential contacts with granule cells would represent a new circuit that is quite unlike that in the cerebellum, in that the cartwheel cells could provide a direct feedback inhibition of granule cell activity. Whether such feedback might represent an on-beam inhibition (with respect to a group of parallel fibers) or a type of spatial lateral inhibition will depend on the relative distribution of contacts with granule cells capable of providing input to a given cartwheel cell vs. contacts with granule cells that contribute parallel fibers running outside the dendritic field of the cartwheel cell. Our results suggest that both patterns of inhibition could exist because the cartwheel cell axons encompass a wider domain in the transstrial axis than their dendritic trees. This axonal distribution is most consistent with that shown for cell II in Berrebi and Mugnaini (1991, Fig. 20A).

A striking feature of the three cells with complete axonal arbors was the planarity of the axonal fields and the coplanar alignment of the dendrites and axons. Both the axonal and the dendritic planes appear to be closely aligned parallel to the isofrequency sheets formed in the deep DCN by the auditory nerve innervation. A similar organization of the axon field was suggested on the basis of anisotropy of PEP-19-stained cells (Berrebi and Mugnaini, 1991). This organizational feature is surprising, because the main excitatory input to the cartwheel cells comes from parallel fibers that run orthogonal to the isofrequency planes; presumably this input does not provide tonotopically organized inputs to cells with dendrites in the molecular layer. Furthermore, deoxyglucose uptake studies (Nudo and Masterton, 1984) have suggested that the molecular layer is not tonotopically organized, because the entire strial extent of the layer is labeled in response to tonal stimulation, whereas there is a discrete tonotopic band in the deeper layers of the nucleus.

The mapping of a nontonotopic organization onto the tonotopic structure of the DCN may have some significant functional consequences. First, the inhibition produced by a single cartwheel cell will be limited to an isofrequency contour by virtue of its flattened axonal arborization. Consequently, only a small set of pyramidal cells will be affected, because they too are highly anisotropic within the isofrequency planes (Blackstad et al., 1984). Thus, the cartwheel cell system maps its own nontonotopic and, perhaps, even a nonauditory input onto a highly frequency-specific region. Second, if cartwheel cells inhibit nearby granule cells, the result will be to prevent the spread of excitation along parallel fibers to other frequency regions. This situation might be important if the granule cells in layer 2 receive any acoustically tuned and tonotopically organized input from the auditory nerve, local interneurons, or descending auditory pathways. The net effect of frequency-specific cartwheel cell inhibition would be suppression of excitation of adjacent frequency domains as mediated by granule cell parallel fibers. The curtailment of such lateral excitation is similar, but not functionally equivalent, to providing lateral inhibition. This pattern of organization might not hold for the granule cell domains outside of the DCN, however, because the cartwheel cell axons do not project into those regions and, thus, cannot be involved in a feedback circuit. Third, the molecular layer itself has an implied tonotopic organization by virtue of the planar dendritic arborizations of both the cartwheel cells and the pyramidal cells. Precisely how these organizational features of the DCN shape the functional properties of the nucleus as a whole remain to be determined.

ACKNOWLEDGMENTS

This paper is based on work supported by NIDCD grants R01 DC00425, K04 DC00048 (P.B.M.), and DC00232 and DC00979 (D.K.R.). Preliminary results of these experiments have been reported in abstract form (Spirou et al., 1991; Manis et al., 1993).

LITERATURE CITED

Berrebi, A.S. and E. Mugnaini (1991) Distribution and targets of the cartwheel cell axon in the dorsal cochlear nucleus of the guinea pig. Anat. Embryol. *183:*427–454.

Berrebi, A.S., J.I. Morgan, and E. Mugnaini (1990) The Purkinje cell class may extend beyond the cerebellum. J. Neurocytol. *19:*643–654.

Blackstad, T.W., K.K. Osen, and E. Mugnaini (1984) Pyramidal neurones of the dorsal cochlear nucleus: A Golgi and computer reconstruction study in cat. Neuroscience *13:*827–854.

Booth, R.F.G., T.B. Patel, and J.B. Clark (1980) The development of enzymes of energy metabolism in the brain of a precocial (guinea pig) and nonprecocial (rat) species. J. Neurochem. *34:*17–25.

Brawer, J.R., D.K. Morest, and E.C. Kane (1974) The neuronal architecture of the cochlear nucleus of the cat. J. Comp. Neurol. *155:*251–300.

Carbone, E. and H.D. Lux (1984) A low voltage-activated, fully inactivating Ca channel in vertebrate sensory neurones. Nature *310:*501–520.

Chen, K., H.J. Waller, and D.A. Godfrey (1993) Cholinergic effects on spontaneous activity of rat dorsal cochlear nucleus neurons. Assoc. for Research in Otolaryngology Abstr. *16:*122.

Crepel, F., and J. Penit-Soria (1986) Inward rectification and low threshold calcium conductance in rat cerebellar Purkinje cells. An in vitro study. J. Physiol. *372:*1–23.

DeCamilli, P., P.E. Miller, P. Levitt, U. Walter, and P. Greengard (1984) Anatomy of cerebellar Purkinje cells in the rat determined by a specific immunohistochemical marker. Neuroscience *11:*761–817.

Disterhoft, J.F., R.E. Perkins, and S. Evans (1980) Neuronal morphology of the rabbit cochlear nucleus. J. Comp. Neurol. *192:*687–702.

Fox, A.P., M.C. Nowycky, and R.W. Tsien (1987) Kinetic and pharmacological properties distinguish three types of calcium currents in chick sensory neurones. J. Physiol. *394:*149–172.

Grace, A.A., and R. Llinás (1985) Morphological artifacts induced in intracellularly stained neurons by dehydration: Circumvention using rapid dimethyl sulfoxide clearing. Neuroscience *16:*461–475.

Hackney, C.M., K.K. Osen, and J. Kolston (1990) Anatomy of the cochlear nuclear complex of guinea pig. Anat. Embryol. *182:*123–149.

Hirsch, J.A., and D. Oertel (1988) Intrinsic properties of neurones in the dorsal cochlear nucleus of mice in vitro. J. Physiol. *396:*535–548.

Horikawa, K., and W.E. Armstrong (1988) A versatile means of intracellular labeling: Injection of biocytin and its detection with avidin conjugates. J. Neurosci. Methods *25:*1–11.

Horner, K.C., J. Serviere, C. Granier-Deferre (1987) Deoxyglucose demonstration of in-utero hearing in the guinea pig foetus. Hearing Res. *26:*327–333.

Kane, E.S. (1974) Synaptic organization in the dorsal cochlear nucleus of the cat: A light and electron microscopic study. J. Comp. Neurol. *155:*301–330.

Kolston, J., K.K. Osen, C.M. Hackney, O.P. Ottersen, and J. Storm-Mathisen (1992) An atlas of glycine- and GABA-like immunoreactivity and colocalization in the cochlear nuclear complex of the guinea pig. Anat. Embryol. *186:*443–465.

Lev-Ram, V., H. Miyakawa, N. Lasser-Ross, and W.N. Ross (1992) Calcium transients in cerebellar Purkinje neurons evoked by intracellular stimulation. J. Neurophysiol. *68:*1167–1177.

Llinás, R. (1988) The intrinsic electrophysiological properties of mammalian neurons: Insights into central nervous system function. Science *242:*1654–1664.

Llinás, R., and C. Nicholson (1971) Electrophysiological properties of dendrites and somata in alligator Purkinje cells. J. Neurophysiol. *34:*534–551.

Llinás, R., and M. Sugimori (1980) Electrophysiological properties of in vitro Purkinje cell somata in mammalian cerebellar slices. J. Physiol. *305:*171–195.

Llinás, R., and Y. Yarom (1981) Properties and distribution of ionic conductances generating electroresponsiveness of mammalian inferior olivary neurones in vitro. J. Physiol. *315:*569–584.

Lorente de Nó, R. (1933) Anatomy of the eighth nerve. III. General plan of structure of the primary cochlear nuclei. Laryngoscope *33:*327–350.

Lorente de Nó, R. (1981) The Primary Acoustic Nuclei. New York: Raven Press.

Manis, P.B. (1989) Responses to parallel fiber stimulation in the guinea pig dorsal cochlear nucleus in vitro. J. Neurophysiol. *61:*149–161.

Manis, P.B. (1990) Membrane properties and discharge characteristics of guinea pig dorsal cochlear nucleus neurons studied in vitro. J. Neurosci. *10:*2338–2351.

Manis, P.B., J.C. Scott, and G.A. Spirou (1993) Physiology of the dorsal cochlear nucleus molecular layer. In M.A. Merchan, J. Juiz, and D.A. Godfrey (eds): The Mammalian Cochlear Nuclei: Organization and Function. New York: Plenum Press, pp. 361–371.

Mason, A., and A. Larkman (1990) Correlations between morphology and electrophysiology of pyramidal neurons in slices of rat visual cortex. II. Electrophysiology. J. Neurosci. *10:*1415–1428.

McCormick, D.A., B.W. Connors, J.W. Lightall, and D.A. Prince (1985) Comparative electrophysiology of pyramidal and sparsely spiny stellate neurons of the neocortex. J. Neurophysiol. *54:*782–806.

Mignery, G.A., T.C. Sudhof, K. Takei, and P. DeCamilli (1989) Putative receptor for inositol 1,4,5-triphosphate similar to ryanodine receptor. Nature *342:*192–195.

Mugnaini, E. (1985) GABA neurons in the superficial layers of the rat dorsal cochlear nucleus: Light and electron microscopic immunocytochemistry. J. Comp. Neurol. *235:*61–81.

Mugnaini, E., and J.I. Morgan (1987) The neuropeptide cerebellin is a marker for two similar neuronal circuits in rat brain. Proc. Natl. Acad. Sci. USA *84:*8692–8696.

Mugnaini, E., K.K. Osen, A.-L. Dahl, V.L. Friedrich, and G. Korte (1980) Fine structure of granule cells and related interneurons (termed Golgi cells) in the cochlear nuclear complex of cat, rat and mouse. J. Neurocytol. *9:*537–570.

Nudo, R.J., and R.B. Masterton (1984) 2-Deoxyglucose studies of stimulus coding in the brainstem auditory system of the cat. In W.D. Neff (ed): Contributions to Sensory Physiology, 8. New York: Academic Press, pp. 79–97.

Oertel, D., and S.H. Wu (1989) Morphology and physiology of cells in slice preparations of the dorsal cochlear nucleus of mice. J. Comp. Neurol. *283:*228–247.

Osen, K.K. (1969) Cytoarchitecture of the cochlear nuclei in the cat. J. Comp. Neurol. *136:*453–483.

Patel, T.B., and J.B. Clark (1980) Comparison of the development of the fatty acid content and composition of the brain of a precocial species (guinea pig) and a nonprecocial species (rat). J. Neurochem. *35:*149–154.

Petralia, R.S., V.A. Trumpy, N.S. Alvanzo, and R.J. Wenthold (1993) Localization of kainate (KA2) and metabotropic (mGLUR1α) glutamate receptors in the cochlear nuclei of the rat using characterized antipeptide antibodies. Assoc. Res. Otolaryngol. Abstr. *16:*120.

Peyret, D., M. Geffard, and J.-M. Aran (1986) GABA immunoreactivity in the primary nuclei of the auditory central nervous system. Hearing Res. *23:*115–121.

Regan, L.J. (1991) Voltage-dependent calcium currents in Purkinje cells from rat cerebellar vermis. J. Neurosci. *11:*2259–2269.

Rhode, W.S., P.H., Smith, and D. Oertel (1983) Physiological response properties of cells labeled intracellularly with horseradish peroxidase in cat dorsal cochlear nucleus. J. Comp. Neurol. *213:*448–463.

Romand, R. (1971) Maturation des potentiels cochlearies dans la periode perinatale chez le chat et chez le Cobaye. J. Physiol. (Paris) *63:*763–782.

Ross, W.N., N. Lasser-Ross, and R. Werman (1990) Spatial and temporal analysis of calcium dependent electrical activity in guinea pig Purkinje cell dendrites. Proc. R. Soc. London [Biol.] *240:*173–185.

Ryugo, D.K., A.H. Sharp, D.D. Wright, and S.H. Snyder (1992) Immunocytochemical localization of the inositol 1,4,5-triphosphate receptor in cartwheel neurons of the mammalian dorsal cochlear nucleus. Assoc. Res. Otolaryngol. Abstr. *15:*76.

Saito, N., U. Kikkawa, Y. Nishizuka, and C. Tanaka (1988) Distribution of protein kinase C-like immunoreactive neurons in rat brain. J. Neurosci. *8:*369–382.

Smith, P.H., and W.S. Rhode (1985) Electron microscopic features of physiologically characterized, HRP-labeled fusiform cells in the cat dorsal cochlear nucleus. J. Comp. Neurol. *237:*127–143.

Spirou, G.A., D.D. Wright, D.K., Ryugo, and P.B. Manis (1991) Physiology and morphology of cells from slice preparations of the guinea pig dorsal cochlear nucleus. Assoc. Res. Otolaryngol. Abstr. *14:*142.

Spirou, G.A., B.J. May, D.D. Wright, and D.K. Ryugo (1993) Frequency organization of the dorsal cochlear nucleus in cats. J. Comp. Neurol. *329:*36–52.

Sugimori, M., and R.R. Llinas (1990) Real time imaging of calcium influx in mammalian cerebellar Purkinje cells in vitro. Proc. Natl. Acad. Sci. USA *86:*5084–5088.

Waller, H.J., and D.A. Godfrey (1991) Functional characteristics of spontaneously active dorsal cochlear nucleus neurons in rat brain. Assoc. Res. Otolaryngol. Abstr. *14:*142.

Waller, H.J., and D.A. Godfrey (1994) Functional characteristics of spontaneously active neurons in dorsal cochlear nucleus in vitro. J. Neurophysiol. *71:*467–478.

Webster, D.B., and D.R. Trune (1982) Cochlear nuclear complex of mice. Am. J. Anat. *163:*103–130.

Wenthold, R.J., J.M. Zempel, K.A. Parakkal, K.A. Reeks, and R.A. Altschuler (1986) Immunocytochemical localization of GABA in the cochlear nucleus of the guinea pig. Brain Res. *380:*7–18.

Wenthold, R.J., D. Huie, R.A. Altschuler, and K.A. Reeks (1987) Glycine immunoreactivity localized in the cochlear nucleus and superior olivary complex. Neuroscience *22:*897–912.

Withington-Wray, D.J., K.E. Binns, and M.J. Eating (1990) The developmental emergence of a map of auditory space in the superior colliculus of the guinea pig. Dev. Brain. Res. *51:*225–236.

Wouterlood, F., and E. Mugnaini (1984) Cartwheel neurons of the dorsal cochlear nucleus: A Golgi-electron microscopic study in rat. J. Comp. Neurol. *227:*136–157.

Wright, D.D., C.D. Blackstone, R.L. Huganir, R.L., and D.K. Ryugo (1993) Immunocytochemical localization of a metabotropic glutamate receptor (mGR1α) within the dorsal cochlear nucleus of the rat. Assoc. Res. Otolaryngol. Abstr. *16:*122.

Zhang, S., and D. Oertel (1993a) Cartwheel and superficial stellate cells of the dorsal cochlear nucleus of mice: Intracellular recordings in slices. J. Neurophysiol. *69:*1384–1397.

Zhang, S., and D. Oertel (1993b) Giant cells of the dorsal cochlear nucleus of mice: Intracellular recordings in slices. J. Neurophysiol. *69:*1398–1408.

Zhang, S., and D. Oertel (1993c) Tuberculoventral cells of the dorsal cochlear nucleus of mice: Intracellular recordings in slices. J. Neurophysiol. *69:*1409–1421.